RESEARCH ARTICLE

Determination of the Permittivity of Transmission Lines at Milli-Kelvin Temperatures

MANOJ STANLEY[1], (Member, IEEE), **ROWAN PARKER-JERVIS**[1,2],
JAMES SKINNER[1], (Member, IEEE), **SEBASTIAN DE GRAAF**[1], **TOBIAS LINDSTRÖM**[1],
JOHN E. CUNNINGHAM[2], **AND NICK M. RIDLER**[1], (Fellow, IEEE)

[1]National Physical Laboratory, TW11 0LW Teddington, U.K.
[2]School of Electronic and Electrical Engineering, University of Leeds, LS2 9JT Leeds, U.K.

Corresponding author: Manoj Stanley (manoj.stanley@npl.co.uk)

ABSTRACT Many quantum technologies rely heavily on propagation of RF and microwave signals through devices at cryogenic temperatures, and detailed understanding of materials and signal propagation is therefore key to improving the performance of quantum circuits. The properties of dielectric substrate materials used for transmission lines (TLs) such as their permittivity need to be precisely determined to design high performance quantum integrated circuits. In this paper, we discuss a measurement technique for determining the effective permittivity of a TL at mK temperatures. The technique utilizes S-parameter measurements of multiple TLs to reliably extract the effective permittivity of the TL implemented in a substrate material. The technique is demonstrated using measured S-parameters of grounded co-planar waveguide (GCPW) at 296 K and 15 mK. The effective permittivity of the TL at 296 K and 15 mK are determined from measurements and compared. We observed the effective permittivity determinations at 15 mK to be approximately frequency independent and calculated the relative permittivity of Rogers RO4350B material at 15 mK to be 3.64. There is no significant deviation from this relative permittivity value with respect to manufacturer data and from measured data at 296 K.

INDEX TERMS Cryogenic temperatures, dilution refrigerator, effective relative permittivity, propagation constant, quantum circuits, transmission line, TRL calibration, vector network analyzer.

I. INTRODUCTION

The continued growth of quantum technologies has created an increasing demand for efficient and well-characterized RF and microwave circuits operating at cryogenic temperatures. The performance and materials of such microwave circuits is important to understand because these can have a significant impact on quantum circuits and the coherence time of quantum bits. The signal propagation in such RF circuitry must have good impedance matching, and spurious signal reflection and loss must be minimized. For this purpose, a detailed knowledge of substrate material properties such as

The associate editor coordinating the review of this manuscript and approving it for publication was Sandra Costanzo.

permittivity at cryogenic temperatures is required in order to design high performance circuits. When cooling to cryogenic temperatures many electrical and physical properties of materials are likely to change, and hence precision measurements must be conducted at low temperatures and ideally in-situ.

The propagation of signals in a transmission line (TL) depends on its propagation constant which in turn is related to the permittivity and permeability of the medium containing the electromagnetic (EM) fields. TLs such as microstrip (MS), and both grounded and ungrounded coplanar waveguide (CPW) are extensively used in integrated circuit technologies, and also in quantum circuits. They provide a low-cost and compact solution with simplicity of fabrication for a dense high frequency system integrated with

both passive and active circuit devices [1]. In such TLs, EM fields lie partly in the air and partly in the dielectric between the conductor and the ground. This complicates the behavior of the EM fields and hence it is usually assumed that the field propagates as a quasi-TEM mode owing to the inhomogeneity in the dielectric medium affecting the EM field distribution. The effective relative permittivity, ε_{reff}, characterizes the behavior of the MS/CPW TL propagation with respect to a homogeneous dielectric medium.

Generally, permittivity characterization techniques can be classified as either resonant or non-resonant techniques. Resonant methods inherently offer higher accuracy owing to the high-quality factors of the resonators being used, which enable a precise determination of the material parameters of a sample placed, for e.g., within a resonant cavity [2] or a printed resonator [3], especially for low-loss materials. By analyzing the variations in the resonator's resonant frequency and quality factor, the complex permittivity of the material under test (MUT) can then be extracted. The applicability of resonator methods is, however, limited to single resonant frequencies of one or more (higher order) modes excited within the resonator, thus offering measurements at only discrete frequencies, while also requiring higher-order mode identification [4], [5]. Often a specialized measurement cell and sample size is required. Such techniques are also not suitable for characterizing dispersive materials whose complex permittivity is highly frequency dependent.

Non-resonant techniques mainly rely on analyzing reflected and/or transmitted electromagnetic waves from the MUT and are normally used to characterize materials over a broad frequency range. A common non-resonant approach is based on TL techniques which have been developed over several decades [6], [7], [8]. Typically, the material is either the substrate of the TL or situated on top of the TL [9], [10]. The propagation constant and characteristic impedance of the TL can be dramatically changed after loading the material. Therefore, by analyzing the variation in the S-parameters of the TL, the change in the propagation constant and the characteristic impedance can be calculated and finally a highly accurate determination of the effective permittivity across a broad frequency band can be obtained.

Generally, when operating and/or characterizing a non-coaxial microwave device under test (DUT) in the form of integrated circuits, the DUT is mounted on a TL implemented on a printed circuit board (PCB) substrate. Specialized TL-based calibration standards containing the same substrate material utilizing the Thru-Reflect-Line calibration algorithm [11] are designed to de-embed calibrated S-parameters of such DUTs. A significant advantage of using a TL-based approach is that these TLs can be exploited to characterize the DUT as well as the substrate material without having to redesign a specialized setup to extract the material properties. Such techniques would be useful in precisely determining material properties at mK temperatures, where material properties are currently not known precisely.

In this paper, a technique is presented to determine ε_{reff} of a TL implemented on a non-magnetic (relative permeability, $\mu_r = 1$) homogeneous substrate material at temperatures down to tens of mK. The technique requires S-parameter measurements of TLs of different lengths. The TLs used in this work have been previously designed to be used as calibration standards to extract calibrated S-parameter measurements of a DUT [12]. These can also be used to extract the material properties of the substrate to which the DUT is mounted. The technique does not require prior knowledge (i.e., an initial or rough estimate) of the propagation constant or relative permittivity of the substrate material which is required for some techniques such as the Nicolson-Ross-Weir Method [13].

The structure of the paper is as follows. Section II describes the generalized equations for extracting ε_{reff} from S-parameters of TLs. This section then describes the design process for the GCPW TLs, which were used for extracting ε_{reff}. The experimental setup to extract ε_{reff} of TLs at 296 K and 15 mK and measurement results are discussed in section III-A and section III-B, respectively. The uncertainty sources associated with these estimations are discussed in section III-C. Some conclusions derived from this work are presented in section IV.

II. PRINCIPLE AND DESIGN

The generalized equations for extracting permittivity from the S-parameters of the TLs along with the design methodology of the PCB-based TLs are discussed in this section.

A. EFFECTIVE PERMITTIVITY FROM S-PARAMETERS

Signal flow graph theory [14] gives the following relations between S-parameters and transmission (T) and reflection (Γ) coefficients:

$$T = \frac{(S_{11} + S_{21}) - \Gamma}{1 - (S_{11} + S_{21})\Gamma} \tag{1}$$

$$\Gamma = K \pm \sqrt{K^2 - 1} \tag{2}$$

where

$$K = \frac{S_{11}^2 - S_{21}^2 + 1}{2S_{11}} \tag{3}$$

The sign in (2) is chosen so that $|\Gamma| \leq 1$, which is required for causal, passive materials.

Assuming that there is a single transverse electromagnetic (TEM) mode of propagation in the TL, the transmission coefficient is given by,

$$T = e^{-\gamma l} \tag{4}$$

where l is the length of the TL.

The propagation constant can be calculated from (4) and is given by:

$$\gamma = -\frac{\ln(T)}{l} = -\frac{1}{l}\left[\ln(|T|) + j\phi_T\right] \tag{5}$$

where ϕ_T denotes the unwrapped phase, and $j^2 = -1$.

The following theory assumes a single TEM wave propagating through the media with a homogeneous cross section. This cannot be satisfied in a straight-forward manner by a planar TL such as a GCPW, since the cross section includes the dielectric substrate below the TL conductors and an air section above the TL conductors. However, most lines of this type can be assumed to support a quasi-TEM mode with effective material parameters modeling a homogeneous cross section, as long as a single mode of propagation is maintained, and higher order modes are sufficiently suppressed. Design rules and methods for avoiding higher order modes in planar TLs such as GCPW and microstrip, have been given by Seiler *et. al.* [15].

To derive the permittivity from the propagation constant, we consider a quasi-TEM wave propagating through a homogeneous, nonmagnetic material. The propagation constant is given as,

$$\gamma = j\frac{\omega}{v} = j\omega\sqrt{\mu_0\varepsilon} = j\omega\sqrt{\mu_0\varepsilon_0\varepsilon_r'\,(1 - j\tan\delta)} \quad (6)$$

where v is the velocity of light inside the material, $\tan\delta$ is the effective loss tangent, and μ_0 and ε_0 are the vacuum permeability and permittivity, respectively. The complex permittivity is given by

$$\varepsilon = \varepsilon' - j\varepsilon'' = \varepsilon_0\varepsilon_r = \varepsilon_0\left(\varepsilon_r' - j\varepsilon_r''\right) \quad (7)$$

where ε_r is the relative permittivity of the material. The primed and double-primed quantities denote the real and imaginary parts of the relative permittivity, respectively.

Since the propagation constant is a complex-valued quantity consisting of an attenuation constant α and a phase constant β, it can also be written as,

$$\gamma = \alpha + j\beta \quad (8)$$

Comparing real and imaginary parts in eq (8) with eq (5) gives,

$$\alpha = -\frac{1}{l}\ln\left(|T|\right) \quad (9)$$

$$\beta = -\frac{1}{l}\left[\phi_T\right] \quad (10)$$

Squaring the propagation constant in (8) and separating it into real and imaginary part results in,

$$Re\left\{\gamma^2\right\} = \alpha^2 - \beta^2 \quad (11)$$

$$Im\left\{\gamma^2\right\} = 2\alpha\beta \quad (12)$$

Combining these equations with (6) and (7), expressions for the real and imaginary parts of the relative permittivity can be obtained as,

$$\varepsilon_r' = -\frac{Re\left\{\gamma^2\right\}}{\omega^2\mu_0\varepsilon_0} = \frac{\beta^2 - \alpha^2}{\omega^2\mu_0\varepsilon_0} \quad (13)$$

$$\varepsilon_r'' = \frac{Im\left\{\gamma^2\right\} - \omega\mu_0\sigma_c}{\omega^2\mu_0\varepsilon_0} \approx \frac{Im\left\{\gamma^2\right\}}{\omega^2\mu_0\varepsilon_0} = \frac{2\alpha\beta}{\omega^2\mu_0\varepsilon_0} \quad (14)$$

where σ_c is the electrical conductivity, $\sigma_c \approx 0$ for low-loss dielectric materials. It is clear by comparing (9)-(10) and (13)-(14), that the real and imaginary parts of the relative permittivity can be estimated if the physical length of the TL is known. However, in the case that the physical length of the TL is not precisely known, there are infinite solutions for the relative permittivity and length; hence, a different approach is required.

In the case of planar TLs exhibiting quasi-TEM propagation, the equations given previously for a homogeneous material can be adapted using the effective permittivity method by simply replacing the relative permittivity, ε_r, by the effective relative permittivity ε_{reff} of the TL's cross section [14], [15].

B. DESIGN OF TRANSMISSION LINE

The Thru-Reflect-Line (TRL) calibration technique can be used to achieve calibrated S-parameter measurements of non-connectorized devices such as RFICs [12], [16], [17] without having the need to precisely characterize all the standards, which is an advantage over techniques such as Short-Open-Load-Thru (SOLT) calibration which requires precise knowledge of all the calibration standards [18]. In [16] and [17], the calibration standards were designed and implemented using GCPW TLs for device calibration at mK temperatures using a 4-wave TRL calibration technique. The propagation constant of the TL can be obtained as a by-product of TRL calibration process. If the physical length of the Line standard is known with respect to the physical length of the Thru standard, then ε_{reff} of the TL can be determined using equations (9)-(14). Utilising multiple TLs of different lengths will enable a more reliable estimation of ε_{reff}. The design process of the TLs used in this work is described in this section.

In [12], the authors designed and implemented a GCPW TL of length 50 mm as the Thru standard so that the middle of the Thru standard was set as the calibration reference plane for the 4-wave TRL calibration. The length of the Thru was chosen to be long enough that the effects of the coaxial connectors and the coaxial to GCPW transitions could be considered to be minimal and for the reference planes to be separated from the plane of interaction of these different effects. The same GCPW Thru standard design is used in this work and is named as "*Line 0*", as shown in Fig. 1.

The Reflect standard is realized as a short-circuit, with two nominally identical short-circuits implemented on a single GCPW PCB, thus providing Reflect standards for both test ports. The reflection coefficient of these short-circuits should be identical for a good quality calibration.

The Line standard consists of an extra section of transmission line that provides a change in the transmission phase, with respect to the Thru connection. The generalized TRL calibration scheme works optimally when the difference in phase between the Thru and the Line standards is $(2n+1)$ $\lambda/4$ and fails completely when this phase difference is
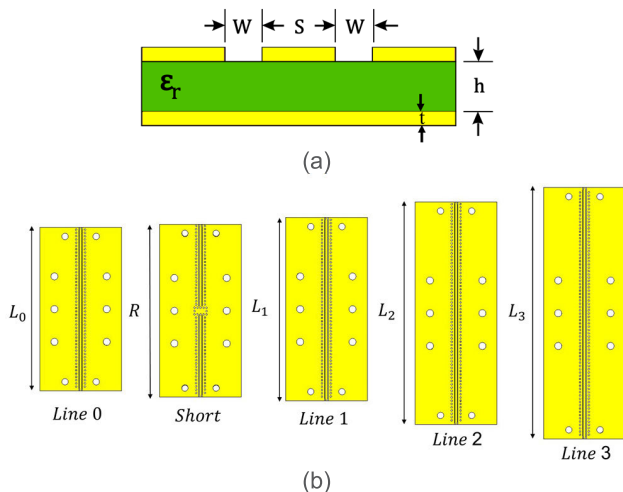
FIGURE 1. (a) Cross section of GCPW TL; (b) GCPW TLs designed to extract ε_{reff}.

TABLE 1. Design parameters for the GCPW TLs.

w	s	h	ε_r	t
0.2 mm	0.7 mm	0.5 mm	3.66	36 μm
R	L_0	L_1	L_2	L_3
52.8 mm	50 mm	56 mm	68 mm	76.8 mm

$(2n)$ $\lambda/4$ (where, $n = 0, 1, 2\ldots$) [19]. Therefore, the line lengths are chosen to prevent phase differences that are close to these calibration failure points. The line standard (*Line 1*) is designed according to the conventional 4-wave TRL calibration technique, to provide a change in the transmission phase, with respect to the Thru connection, of approximately $90° - i.e.,$ 4-wavelength – at frequencies around the middle of the frequency range of interest. The calibration failure points will occur at phase changes of 0° and 180°. Therefore, when designing line standards for a 4-wave TRL calibration procedure, phase changes are designed to be within 20° and 160°, i.e., at least 20° greater than 0° and at least 20° less than 180° [19]. Therefore, a single line standard is designed to be 6 mm (4 of the GCPW wavelength at 8 GHz) longer than the Thru standard and so is suitable for covering the frequency range of 1.8-14 GHz.

Two additional transmission lines (*Line 2* and *Line 3*) were designed in [12] to be used as line standards to implement a $\frac{3}{4}$-wave TRL calibration as an independent calibration technique to validate S-parameter measurements at mK temperatures. In this work, these additional TLs are utilised as DUT TLs instead of line standards to provide redundancy in the measurements allowing a statistical approach to be applied for extraction of the effective relative permittivity as will be discussed later. The detailed design parameters for the length of both these transmission lines to use them as $\frac{3}{4}$-wave TRL calibration standards are given in [12] and so will not be discussed in this paper.

Rogers RO4350B with relative permittivity 3.66 and loss tangent 0.0037 at 10 GHz at room temperature was used as the PCB substrate for all the TL designs. The top and bottom copper ground planes of 1.4 mil (≈ 36 μm) thickness are connected by using metallized via holes of 0.5 mm diameter. The initial dimensions of the GCPW structure (such as the center conductor width, the gap width between the center conductor and the two grounds, and substrate thickness) were

estimated by solving the simplified frequency independent analytical equations in [20] for a characteristic impedance of 50 Ω.

$$Z_0 = \frac{60\pi}{\sqrt{\varepsilon_{reff}}} \frac{1}{\frac{K(k)}{K(k')} + \frac{K(k1)}{K(k1')}} \tag{15}$$

$$k = \frac{s}{s + 2w} \tag{16}$$

$$k' = \sqrt{1 - k^2} \tag{17}$$

$$k1' = \sqrt{1 - k1^2} \tag{18}$$

$$k1 = \frac{\tanh\left(\frac{\pi s}{4h}\right)}{\tanh\left(\frac{\pi(s+2w)}{4h}\right)} \tag{19}$$

$$\varepsilon_{reff} = \frac{1 + \varepsilon_r \frac{K(k')}{K(k)} \frac{K(k1)}{K(k1')}}{1 + \frac{K(k')}{K(k)} \frac{K(k1)}{K(k1')}} \tag{20}$$

where Z_0 is the characteristic impedance of the GCPW transmission line, s is the track width of the GCPW TL, w is the gap width, h is the height of the substrate material and $K(k)$ is an elliptical integral of the first kind and is calculated using recursive equations in [21].

These initial dimensions were used to model and design the GCPW TLs using CST Microwave Studio. Coaxial-to-GCPW transitions were added to the ends of the PCB standards to ensure radiation-free wave propagation, and hence minimize any degradation in the calibration. The optimised designs of the TL standards were simulated in CST Design Studio and their S-parameters investigated to ensure the simulated performance was acceptable in terms of impedance matching and insertion loss. The final design dimensions and parameters used for all the GCPW TLs are given in Table 1.

C. TECHNIQUE TO EXTRACT EFFECTIVE RELATIVE PERMITTIVITY

In practice, the TLs described in the previous section will be fitted with coaxial connectors after fabrication to facilitate connection to a Vector Network Analyzer (VNA) to record the S-parameter measurements at 296 K and 15 mK. Coaxial to GCPW transitions are therefore added to the PCB to ensure adequate impedance matching between the GCPW TL and the coaxial connectors, thus avoiding any unwanted effects due to non-TL modes affecting the S-parameter measurements. It becomes, therefore, necessary to apply a calibration sequence, to de-embed connector effects from the measured S-parameters of the TLs to extract the ε_{reff}

precisely. This calibration sequence is described in this section.

Combining (9), (10) and (13) for a GCPW TL gives,

$$\varepsilon'_{reff}(f) = \frac{[\phi_T(f)]^2 - \ln(|T(f)|)^2}{l^2 \omega^2 \mu_0 \varepsilon_0} \quad (21)$$

For a well-matched TL, $T \to S_{21}$, (21) becomes,

$$\varepsilon'_{reff}(f) = \frac{[\phi_{S_{21}}(f)]^2 - \ln(|S_{21}(f)|)^2}{l^2 \omega^2 \mu_0 \varepsilon_0} \quad (22)$$

Similarly combining (9), (10) and (14) gives,

$$\varepsilon''_{reff}(f) = \frac{(\phi_{S_{21}}(f)) \times \ln(|S_{21}(f)|)}{l^2 \omega^2 \mu_0 \varepsilon_0} \quad (23)$$

The technique will be illustrated by extracting the frequency dependent real part of the effective relative permittivity, $\varepsilon'_{reff}(f)$. However, it can also be utilized to extract the imaginary part, $\varepsilon''_{reff}(f)$. The designed TLs *Line 0*, *Line 1*, *Line 2* and *Line 3* are used to generate three independent equations as explained below.

The first equation is generated by utilizing *Line 0* of length L_0 (as labelled in Fig. 1) as a Thru standard, *Line 1* of length L_1 as a Line standard, *Short* as reflect standards. After the application of TRL calibration, the calibrated S-parameters with *Line 1* as a DUT will correspond to a TL section of physical length of approximately $len_1 = L_1 - L_0$, i.e. the difference in length between the DUT and the Thru standard. The ε'_{reff} of the calibrated TL section of length len_1 is given as,

$$\varepsilon'_{reff,1}(f) = \frac{[\phi_{S_{21,1}}(f)]^2 - \ln(|S_{21,1}(f)|)^2}{len_1^2 \omega^2 \mu_0 \varepsilon_0} \quad (24)$$

For simplicity, we assign $a_1 = \phi_{S_{21,1}}(f)$ and $b_1 = \ln(|S_{21,1}(f)|)$, which gives,

$$\varepsilon'_{reff,1}(f) = \frac{a_1^2 - b_1^2}{len_1^2 \omega^2 \mu_0 \varepsilon_0} \quad (25)$$

where a_1 and b_1 correspond to the unwrapped phase and magnitude of the transmission coefficient of the TL section of length len_1, respectively.

Two other equations can be generated in the same way by utilizing *Line 2* and *Line 3* TLs as DUTs.

The resulting equations can be summarized as:

$$\varepsilon'_{reff,k}(f) = \frac{a_k^2 - b_k^2}{len_k^2 \omega^2 \mu_0 \varepsilon_0} \quad (26)$$

where k=1,2,3 indicate the respective *Line k* TL.

In (26), the 'a' and 'b' terms are known following the above calibration processes from the measured S-parameters of the TLs. The 'len_k' for each of the TLs is determined from dimensional measurements at room temperature. At mK temperatures, a correction factor is applied to these room
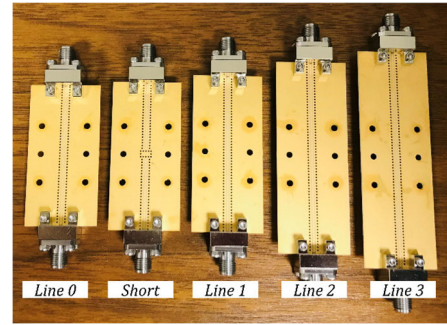

FIGURE 2. Connectorized TLs.

temperature measurements to accommodate for thermal contraction. Based on the reported thermal expansion coefficient of copper $11 \times 10^{-6} K^{-1}$ [22], we calculate the contraction in the length of TLs to be 0.4% when cooling from 296 K to 15 mK using the below equation.

$$\alpha_L = \frac{1}{L} \frac{dL}{dT} \quad (27)$$

where α_L is the coefficient of thermal contraction, dT is the change in temperature from 296 K to 15 mK, dL is the change in estimated length of TL from 296 K to 15 mK, L is the measured length of TL at 296 K. Although the thermal coefficient of expansion/contraction is likely to be a non-linear function of temperature, in this case (27) provides a linear, first order approximation.

$$\varepsilon'_{reff} = \sum_{k=1}^{k=3} \varepsilon'_{reff,k}(f)/3 \quad (28)$$

The $\varepsilon'_{reff,k}$ is calculated using (26) and averaged to determine the ε'_{reff} of the TL. We will limit the measurements to 4-12 GHz for the discussions in this paper, since the subsequent cryogenic measurements at 15 mK were band-limited as a result of specialized narrowband amplifiers and directional couplers used inside the dilution refrigerator as discussed in section III-B.

III. ESTIMATION OF EFFECTIVE RELATIVE PERMITTIVITY FROM MEASURED S-PARAMETERS
A. ROOM TEMPERATURE SETU

The TLs were fabricated using an Electroless Palladium Autocatalytic Gold (EPAG) process with Copper coated with Gold plating which is non-magnetic (Nickel free) and suitable for wire bonding. Solder free contact based 3.5 mm edge-launch coaxial connectors were then connected to both ends of all the TLs, as shown in Fig. 2, to facilitate subsequent connection to a vector network analyzer (VNA). The physical length of the TLs was measured using a micrometer, by comparison with gauge blocks with SI traceable calibration of uncertainty of 0.3 μm, as shown in Fig. 3. The length measurement was taken on both the left and right sides of each of the TL, along the longer edge, as shown
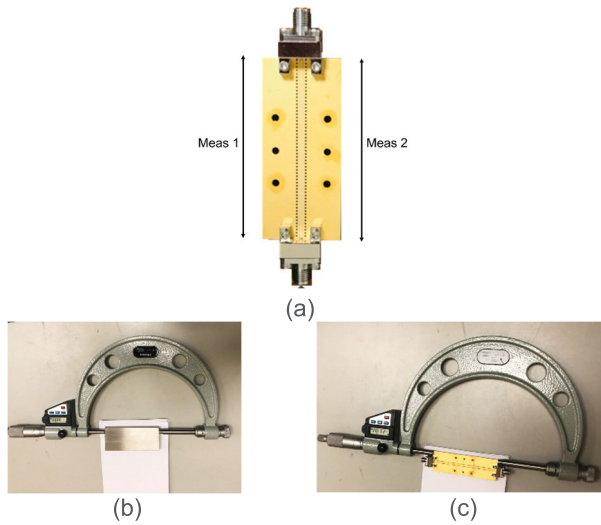
FIGURE 3. (a) Illustration of dimensional measurements taken; (b) calibration measurement using gauge blocks and (c) length measurement of TL.
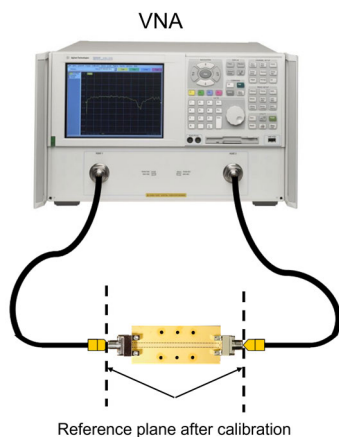

FIGURE 4. S-parameter measurement setup at room temperature with one of the TLs connected to the VNA.

TABLE 2. Physical length of TLs from dimensional measurements.

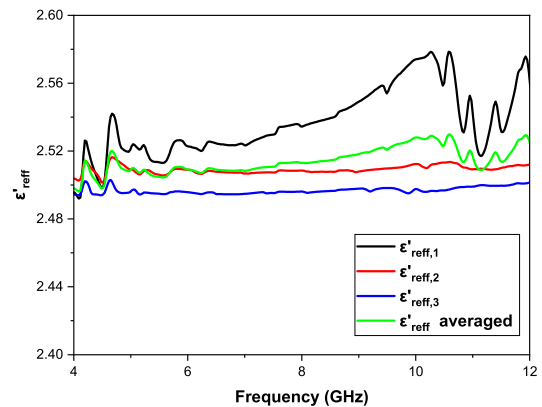| Measurement	Line 0 (mm)	Line 1 (mm)	Line 2 (mm)	Line 3 (mm)
Meas 1	50.166	56.050	68.136	76.929
Meas 2	50.173	56.068	68.118	76.904
Average	50.1695	56.059	68.127	76.9165
Design length	50	56	68	76.8
Fabrication error (%)	0.34	0.11	0.19	0.15

FIGURE 5. Extracted ε'_{reff} from measured data of TLs at 296 K.

In the next step, an offline TRL calibration was performed to enable S-parameter measurements of the TLs, as discussed in section II-C. This is to remove the effects of the coaxial connectors and coaxial to GCPW transitions and generate the equations in (26) to extract ε'_{reff}. In all these equations, the 'a' and 'b' terms are determined from the measured S-parameters of the TLs at 296 K. The ε'_{reff} was found to be approximately independent of frequency and therefore, was averaged to be 2.51 at 296 K. The $\varepsilon'_{reff,k}$ calculated from each of the TLs along with the averaged ε'_{reff} is plotted in Fig. 5. The ε'_{reff} determined using *Line 1* has the highest deviation from the averaged ε'_{reff} due to the shorter length of the line.

B. CRYOGENIC TEMPERATURE SETUP

The fabricated TLs were deployed inside a dilution refrigerator for operation at mK temperatures, a schematic of the cryogenic microwave setup is shown in Fig. 6. The TLs were selected by two software controlled SP6T RF switches driven at mK temperatures via DC wiring [12], [16], [17]. The TLs were connected to the RF switch port of each of the RF switches using phase-matched 3.5 mm coaxial cables. In this set-up, all four uncalibrated S-parameters are obtained by activating and measuring the respective input and output coaxial paths, connecting the TLs to the VNA test ports through two SPDT switches operating at room temperature. Attenuators were added in the input path at different stages to thermalize cables and reduce incoming thermal radiation to a level compatible with superconducting

in Fig. 3(a) to account for imperfections in manufacturing process and then averaged for each of the TLs as shown in Table 3.

The fabricated TLs were then characterized at room temperature using an Agilent E8364C VNA as shown in Fig. 4. A Short-Open-Load-Reciprocal Thru (SOLR) calibration was applied using the VNA firmware to bring the reference plane of the measurements to the ends of the test cables, as shown in Fig. 14, enabling the S-parameters of the TLs to be determined. These room temperature measurements were made to ensure that the performance of the TLs was not compromised due to any fabrication errors or issues due to the edge launch coaxial connectors. The calibration standards were traceable, pre-characterised Short-Open-Load standards from a Maury Microwave 3.5mm calibration kit, along with an "unknown reciprocal thru" adaptor.

FIGURE 6. Block diagram of the cryogenic S-parameter set-up used to extract ε_{reff} [12].

FIGURE 7. Cryogenic S-parameter set-up inside the dilution refrigerator to extract ε_{reff} z of the TLs at mK temperatures.

quantum circuits [23]. The cryogenic directional couplers operating from 4-12 GHz were connected as close to the TLs as possible to bring the VNA receivers from room temperature stage to mK temperature stage, closer to the TL plane. The directional couplers limit the frequency range of operation for mK measurements over which ε'_{reff} can be extracted. However, wider bandwidth directional couplers are commercially available if the material properties are required over a wider frequency range. Low noise amplifiers (LNAs) operating from 0.5-14 GHz were added to the output paths to amplify the signal levels to an acceptable level for VNA measurements. The S-parameter measurement set-up containing the TLs inside the coldest stage (< 20 mK) of the dilution refrigerator is shown in Fig. 7.

To extract ε'_{reff} at mK temperatures, in the first step, the raw S-parameter data for all the TLs were recorded at
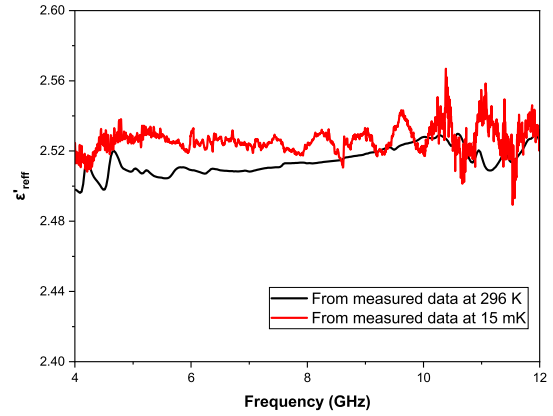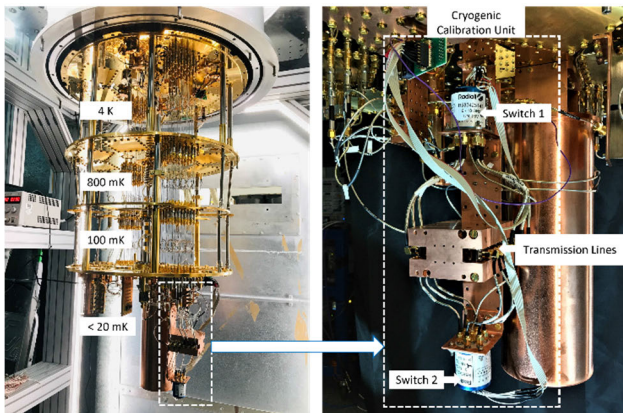

FIGURE 8. Comparison of ε'_{reff} from measurement results at room temperature and cryogenic temperature.

TABLE 3. Comparison of calculated ε_r z.

	ε_r
From measured data at 296 K	3.62
From measured data at 15 mK	3.64
From manufacturer data	3.66

mK temperature using the VNA by controlling the SP2T and SP6T switches operating at room temperature and mK temperature, respectively. Then a TRL calibration was applied to the data recorded at mK temperatures using the calibration standards as discussed in section II-C, to extract the $\varepsilon'_{reff,k}$ using the same method as at room temperature. For the mK measurement, we use the measured room temperature TL lengths, len_k, with a 0.4% reduction in length to account for thermal contraction [22]. The average ε'_{reff} obtained at mK is plotted in Fig. 8 and compared to the room temperature measurement. The ε'_{reff} was observed to be approximately frequency independent and therefore averaged across the frequency range to obtain a value of 2.52 at 15 mK. Hence, there is no detectable deviation in ε'_{reff} of TLs implemented in Rogers 4350B at 15 mK compared to room temperature.

The frequency independent ε'_{reff} values at 296 K and 15 mK have been used to estimate the relative permittivity (ε_r) using equations (16)-(20). The value of ε''_{reff} is calculated to be negligibly small and therefore $\varepsilon_{reff} \approx \varepsilon'_{reff}$ in (20). The value of TL dimensions (s, w, and h) at 296 K are based on design dimensions. The value of TL dimensions at 15 mK have been modified using the correction factor to include contraction of dimensions as temperature goes down from 296 K to 15 mK. It is to be noted that for all these calculations, the coefficient of thermal contraction is assumed to be uniform in all directions, although, in practice there will be some minor anisotropy. The calculated ε_r values at 296 K and 15 mK are summarised in Table. 3 along with manufacturer's ε_r value [24]. The estimated ε_r at 296 K and 15 mK deviates from the manufacturer's data by about 1% and 0.5% respectively.

C. SOURCES OF UNCERTAINTY

The measurements at 296 K will have errors due to the VNA. Although, systematic errors can be mathematically corrected to a large extent by the calibration process, random errors and drift errors cannot be eliminated. However, these can be minimized by taking appropriate measures, for example, averaging and reduced IF bandwidth can minimize random errors due to noise and performing measurements in a controlled environment can reduce drift errors. Another potential source of error can be attributed to the movement of test cables while connecting different TLs. This could be reduced by using higher quality rigid cables with good phase stability. An implicit assumption is that the material properties of the substrate material used in all the TLs are identical. However, they can in fact vary, especially if the substrate materials were fabricated in different batches under different conditions. There are also variations between the edge launch coaxial connectors due to fabrication tolerances as well as differences resulting from connection repeatability to the coaxial-to-GCPW transitions on the TLs. One way to minimize this is to carefully mount the connectors to the TLs and check alignment using a microscope to ensure that a similar connection is made between the connector pin and the PCB for all TLs.

For the measurement setup at mK temperatures, all aspects of the setup from the room temperature VNA down to the low temperature RF switches is accounted for in the error model during calibration. The cryogenic RF switch ports and the cables connecting the RF switches to the TLs need to be as identical as possible at mK temperatures to minimize calibration errors. The RF switch ports can create differences in transmission paths and return losses intrinsic to the switches. The variability and repeatability of the RF switch ports have been investigated in [17]. Reference plane errors due to RF cables connecting the TLs to the RF switches can be minimized by phase-matching the cables at room temperature. However, the temperature related effects on each cable may be different depending on the bending of the cables which is dictated by the physical length of the TL to which it is connected [17]. To estimate the variability and repeatability of the RF switch ports and the variability of cables at mK temperatures, the RF switches along with the cables need to be characterized in detail. As the RF switches are coaxial devices, an S-parameter measurement setup employing coaxial calibration standards similar to [25] will need to be utilized to measure the calibrated S-parameters of RF switches. This is work that is on-going and will be reported in a future publication.

During the extended period of the measurement cycle, any drift occurring due to temperature changes inside and outside the dilution refrigerator will introduce errors in calibration. Cable movements at room temperature can also introduce errors. The variations at room temperature can create drift in the amplifier stage, cables, and the VNA. By regularly re-calibrating the measurement system, these errors can be reduced.

IV. CONCLUSION

This paper has introduced a measurement technique to determine the permittivity of a TL using S-parameters of multiple TLs of different lengths at mK temperatures. This will prove beneficial for quantum technologies, for example, for quantum computing systems operating at cryogenic temperatures, where effective relative permittivity of TLs is not precisely known. The technique has been demonstrated using measured S-parameters of GCPW TLs as an example at 296 K and 15 mK. Although the technique was demonstrated using GCPW TLs, it can also be utilized for other types of TLs such as microstrip, CPW, Goubau lines, etc.

REFERENCES

[1] W. R. Deal, "Coplanar waveguide basics for MMIC and PCB design," *IEEE Microw. Mag.*, vol. 9, no. 4, pp. 120–133, Aug. 2008.

[2] J. Ma, Z. Wu, Q. Xia, S. Wang, J. Tang, K. Wang, L. Guo, H. Jiang, B. Zeng, and Y. Gong, "Complex permittivity measurement of high-loss biological material with improved cavity perturbation method in the range of 26.5–40 GHz," *Electronics*, vol. 9, no. 8, p. 1200, Jul. 2020.

[3] A. Raveendran and S. Raman, "Complex permittivity extraction of planar dielectrics using a noninvasive microwave transmission line resonant technique," *IEEE Trans. Instrum. Meas.*, vol. 70, pp. 1–8, 2021.

[4] J. Krupka, W. Gwarek, N. Kwietniewski, and J. G. Hartnett, "Measurements of planar metal–dielectric structures using split-post dielectric resonators," *IEEE Trans. Microw. Theory Techn.*, vol. 58, no. 12, pp. 3511–3518, Dec. 2010.

[5] H. B. Wang and Y. J. Cheng, "Broadband printed-circuit-board characterization using multimode substrate-integrated-waveguide resonator," *IEEE Trans. Microw. Theory Techn.*, vol. 65, no. 6, pp. 2145–2152, Jun. 2017.

[6] M. D. Janezic and D. F. Williams, "Permittivity characterization from transmission-line measurement," in *IEEE MTT-S Int. Microw. Symp. Dig.*, Denver, CO, USA, Jun. 1997, pp. 1343–1346.

[7] M. D. Janezic, D. F. Williams, V. Blaschke, A. Karamcheti, and C. S. Chang, "Permittivity characterization of low-k thin films from transmission-line measurements," *IEEE Trans. Microw. Theory Techn.*, vol. 51, no. 1, pp. 132–136, Jan. 2003.

[8] K. Grenier, D. Dubuc, P.-E. Poleni, M. Kumemura, H. Toshiyoshi, T. Fujii, and H. Fujita, "Integrated broadband microwave and microfluidic sensor dedicated to bioengineering," *IEEE Trans. Microw. Theory Techn.*, vol. 57, no. 12, pp. 3246–3253, Dec. 2009.

[9] F. Costa, M. Borgese, M. Degiorgi, and A. Monorchio, "Electromagnetic characterisation of materials by using transmission/reflection (T/R) devices," *Electronics*, vol. 6, no. 4, p. 95, Nov. 2017.

[10] U. C. Hasar and C. R. Westgate, "A broadband and stable method for unique complex permittivity determination of low-loss materials," *IEEE Trans. Microw. Theory Techn.*, vol. 57, no. 2, pp. 471–477, Jan. 2009.

[11] G. F. Engen and C. A. Hoer, "Thru-reflect-line: An improved technique for calibrating the dual six-port automatic network analyzer," *IEEE Trans. Microw. Theory Techn.*, vol. MTT-27, no. 12, pp. 987–993, Dec. 1979.

[12] M. Stanley, R. Parker-Jervis, S. de Graaf, T. Lindström, J. E. Cunningham, and N. M. Ridler, "Validating S-parameter measurements of RF integrated circuits at milli-Kelvin temperatures," *Electron. Lett.*, vol. 58, no. 16, pp. 614–616, Aug. 2022.

[13] A. M. Nicolson and G. F. Ross, "Measurement of the intrinsic properties of materials by time-domain techniques," *IEEE Trans. Instrum. Meas.*, vol. IM-19, no. 4, pp. 377–382, Nov. 1970.

[14] P. Seiler and D. Plettemeier, "A method for substrate permittivity and dielectric loss characterization up to subterahertz frequencies," *IEEE Trans. Microw. Theory Techn.*, vol. 67, no. 4, pp. 1640–1651, Apr. 2019.

[15] P. Seiler, B. Klein, and D. Plettemeier, "Analytical and experimental investigation of substrate permittivity and loss up to 67 GHz," in *Proc. 20th Asia–Pacific Conf. Commun. (APCC)*, Oct. 2014, pp. 123–128.

[16] M. Stanley, S. E. de Graaf, T. Lindström, M. J. Salter, J. Skinner, and N. M. Ridler, "Design of microwave calibration standards for characterising S-parameters of quantum integrated circuits at millikelvin temperatures," in *Proc. 51st Eur. Microw. Conf.*, Apr. 2022, pp. 639–642.

[17] M. Stanley, S. De Graaf, T. Hönigl-Decrinis, T. Lindström, and N. M. Ridler, "Characterizing scattering parameters of superconducting quantum integrated circuits at milli-Kelvin temperatures," *IEEE Access*, vol. 10, pp. 43376–43386, 2022.

[18] A. Rumiantsev and N. Ridler, "VNA calibration," *IEEE Microw. Mag.*, vol. 9, no. 3, pp. 86–99, Jun. 2008.

[19] N. M. Ridler, "Choosing line lengths for calibrating waveguide vector network analysers at millimetre and sub-millimetre wavelengths," Nat. Phys. Lab., Teddington, U.K., Tech. Rep. TQE 5, Mar. 2009.

[20] B. C. Wadell, *Transmission Line Design Handbook*. Norwood, MA, USA: Artech House, 1991, p. 79.

[21] H. C. Miller, "Inductance formula for a single-layer circular coil," *Proc. IEEE*, vol. 75, no. 2, pp. 256–257, Feb. 1987.

[22] N. J. Simon, E. S. Drexler, and R. P. Reed, "Properties of copper and copper alloys at cryogenic temperatures," NIST Monograph, Boulder, CO, USA, Tech. Rep. 177, Feb. 1992.

[23] P. Krantz, M. Kjaergaard, F. Yan, T. P. Orlando, S. Gustavsson, and W. D. Oliver, "A quantum engineer's guide to superconducting qubits," *Appl. Phys. Rev.*, vol. 6, no. 2, Jun. 2019, Art. no. 021318.

[24] *RO4000 Series High Frequency Circuit Materials*. Accessed: Mar. 2023. [Online]. Available: https://www.mclpcb.com/wp-content/uploads/2021/05/Rogers-ro4000-laminates-ro4003c-and-ro4350b-data-sheet.pdf

[25] J. Skinner, M. Stanley, J. Urbonas, S. de Graaf, T. Lindström, and N. Ridler, "Characterizing precision coaxial air lines as reference standards for cryogenic S-parameter measurements at milli-Kelvin temperatures," in *IEEE MTT-S Int. Microw. Symp. Dig.*, Jun. 2023.

JAMES SKINNER (Member, IEEE) joined the U.K.'s National Physical Laboratory, Electromagnetic Measurements Group, in 2016. He specializes in impedance metrology and VNA calibration. He is currently involved in the maintenance of primary national standards for impedance measurements and the maintenance and development of traceability to the SI for S-parameter measurement systems operating at frequencies ranging from a few kHz to sub-THz.

SEBASTIAN DE GRAAF is currently with the National Physical Laboratory.

TOBIAS LINDSTRÖM is currently with the National Physical Laboratory.

JOHN E. CUNNINGHAM received the B.Sc. degree from University College London, in 1995, the M.Sc. degree from the Imperial College London, in 1996, and the Ph.D. degree from the University of Cambridge, in 2000. Since then, he has held both EPSRC and Royal Academy of Engineering Fellowships and has been the Deputy Head of the School of Electronic and Electrical Engineering, University of Leeds, since 2016. He has been directed the U.K. network for terahertz science and technology Teranet, since 2017. His research interests include cryogenic high frequency measurements and their use for measurements in condensed matter physics and the development of new applications of GHz to THz measurements techniques across the fundamental sciences.

MANOJ STANLEY (Member, IEEE) received the Ph.D. degree in electrical engineering from the University of Liverpool, in 2019. Currently, he is with the U.K.'s National Physical Laboratory, Electromagnetic Technologies Group, as a Senior Research Scientist. He has led and supported the development of next-generation computing and communications technologies and high-frequency electronics applications. He is also developing high-frequency metrology capabilities to characterize quantum and microwave devices at cryogenic temperatures for quantum computing applications.

ROWAN PARKER-JERVIS received the joint Ph.D. degree in electronic engineering from the National Physical Laboratory and the University of Leeds, in 2022. Currently, he is with the BAE Systems in the Training Services Group as a Model Based Systems Engineer. Alongside this, he is an Officer with Army Reserve, where he leads a troop of Royal Engineers.

NICK M. RIDLER (Fellow, IEEE) received the B.Sc. degree from the King's College London, University of London, London, U.K., in 1981. He is currently the Head of Science with the U.K.'s National Physical Laboratory (NPL), Electromagnetic and Electrochemical Technologies Department. He is also a NPL Fellow and an Honorary Professor with the University of Glasgow and University of Liverpool, U.K., and a Visiting Professor with the University of Kent, University of Leeds, and University of Strathclyde, U.K. He is also the Non-Executive Director of LA Techniques Ltd., and a fellow of the Institution of Engineering and Technology (IET) and the Institute of Physics (IOP). He has more than 35 year's experience working in industrial, government, and academic research establishments. His research interest includes precision high-frequency electromagnetic measurement (from 1 kHz to 1 THz).

. . .